PROCEEDINGS A

royalsocietypublishing.org/journal/rspa

Research

Article submitted to journal

Subject Areas:
fluid mechanics, applied mathematics

Keywords:
hydrogels, freeze fracturing, poroelasticity

Author for correspondence:
Joseph J. Webber
e-mail: joe.webber@warwick.ac.uk

THE ROYAL SOCIETY
PUBLISHING

Cryosuction and freezing hydrogels

Joseph J. Webber[1] and M. Grae Worster[2]

[1] Mathematics Institute, University of Warwick, Coventry CV4 7AL, UK
[2]Department of Applied Mathematics and Theoretical Physics, Centre for Mathematical Sciences, Wilberforce Road, Cambridge CB3 0WA, UK

Recent experiments have shown a rich variety of behaviour when soft, brittle, hydrogels are frozen, since water cannot freeze within the pore space of these materials as a result of the Gibbs-Thompson effect. Hence, no ice forms within the hydrogel matrix, and pure ice grows by cryosuction, drawing water from the surrounding gel towards the phase boundary. The growth of this ice leads to deformation of the poroelastic gel, and drives interstitial flows in the nanoscale pores within the remaining dried hydrogel. In this paper, we model the formation of ice when hydrogels are cooled at a fixed surface, and investigate both the rate at which the ice grows and the elastic response of the gel that remains, explaining the steady states seen in experiments and the processes by which damage can be effected on the hydrogel. Understanding these freezing behaviours is vitally important if we are to comprehend the mechanisms behind damage to porous media such as asphalt road surfaces or human organs when they are frozen, and how to mitigate such effects.

1. Introduction

Hydrogels comprise an elastic, hydrophilic, polymer scaffold saturated with adsorbed water molecules that are free to move through the porous structure formed by the cross-linked polymer chains. When such gels are brought below the freezing point of water, a complicated range of phenomena – ranging from the formation of ice lenses [1] to mushy layers [2] – are observed. Common to these phenomena is the fact that water cannot easily freeze within the pores of a hydrogel unless the temperature is very low, since the ice-entry temperature of the pore space is significantly below the freezing point of bulk water. This effect is well-known,

arising from capillarity, and is described extensively in the literature [3–5].

The Gibbs-Thompson effect lowers the freezing temperature of water at curved interfaces to a value

$$T_{\text{ice-entry}} = T_m - \Gamma\kappa, \tag{1.1}$$

where T_m is the unconfined melting point, κ is the curvature and $\Gamma = \gamma T_m/\rho_s\mathcal{L}$ [4] is a positive parameter related to the surface tension γ, the solid (ice) density ρ_s and the specific latent heat of fusion $\mathcal{L}$. In the case of a hydrogel, the curvature κ would scale with the reciprocal of the pore scale of 10^{-8} to 10^{-7} m [6] and therefore the ice-entry temperature will be of the order $-10\,^\circ$C or lower.

Therefore, at moderately cold temperatures below freezing but above the ice-entry temperature, ice will form separate from the gel, and water must be drawn from the hydrogel to form this ice. This process, where water is driven from the hydrogel and sucked into the growing ice, is referred to as 'cryosuction' [7], and leads to the deswelling or 'drying' of the remaining gel. Modelling the freezing process therefore requires a coupling between the thermal effects involved in freezing itself and the elastic and osmotic effects driving flow and reconfiguration of the hydrogel matrix as water is removed.

When ice forms in soft, wet, porous materials such as soils or plant tissues, predicting its form and growth patterns can be incredibly complicated. As a result, many models of such processes are empirical in nature [8], and research into frost damage has tended to progress independently in biology [9], plant physiology [10] and food science [11], even though the underlying physical processes are identical. It is also commonly reported that brittle materials are damaged primarily by the volumetric expansion of water as it freezes into ice, but this has been shown definitively not to be the case. Since water expands by only around 10% in volume when freezing into ice, this leads to strains of the order of 2% in each direction, often well within the range of strain easily accommodated by elastic media without damage [7,8]. Instead, it is the process of cryosuction, and the draw of water from wetter regions to form the ice, that causes the damage in the freezing process [7], since the growing ice displaces the bulk material, resulting in stresses that cannot be supported without fracture. Indeed, damage still occurs when there is no expansion upon freezing, and liquids that contract when they freeze exhibit buildups of stress [12].

A number of experiments have been carried out in recent years to illustrate this phenomenon [1,7,13], measuring stress buildup in gels as ice forms. In this paper, we couple a model for the formation of ice to the linear-elastic-nonlinear-swelling (LENS) theory for hydrogels introduced in recent studies [14,15] to explain the physical origin of these stresses. We start by introducing boundary conditions at the ice–gel phase boundary, and quantify the depression in freezing temperature as a function of the osmotic pressure in the gel. Coupling this with a Stefan condition that sets the rate at which water must be drawn from the hydrogel to form ice, we are able to model the growth of an ice layer and the evolution of the gel composition that results.

As a first application of this modelling, we will explain the one-dimensional growth of ice at a cooled boundary investigated experimentally in [1,16]. In these experiments, ice is seen to grow and water is drawn from the hydrogel until a steady state is reached comprising a finite thickness ice layer and partially-dried gel. We show that this state occurs when the temperature of the cooled boundary matches the liquidus temperature, so that the thickness of the ice in steady state measures the osmotic pressure in the hydrogel (an example of gel-freezing osmometry, or GelFrO [16]). Furthermore, our modelling allows for the investigation of the transient state, including how the growth rate of ice depends on material properties and temperature differences.

Secondly, we extend our modelling to a two-dimensional system akin to that explored experimentally in [1]. Here, the lower boundary of a narrow channel of gel is cooled with a temperature gradient, with a thicker layer of ice forming in the cooler regions and no ice forming on sections of the boundary at a temperature above the unmodified freezing temperature of water. In this case, in addition to the flow directly towards the phase boundary, there is interstitial flow from the warmer, more swollen gel towards the colder, drier regions until a steady state is reached in which osmotic pressures balance deviatoric stresses due to differential swelling in the gel.

This modelling allows us to understand the source of stress buildup at the ice–gel boundary and the specific way in which the surrounding elastic matrix must deform. We can derive analytical expressions for the displacement field and the strains in the dried hydrogel, giving an explanation for the effect of boundary conditions on the mode of damage first seen experimentally by [1].

2. Equations and boundary conditions governing freezing

In a recent series of papers, we introduced a model for the dynamics of super-absorbent gels founded on a linear-elastic constitutive relation that allows for large isotropic deformation corresponding to swelling or drying [14,15], in effect treating a hydrogel swollen to any degree as a linear-elastic material whose properties change based on the amount of water within the pore space. Relative to a reference state in which a gel is fully swollen with a uniform polymer volume fraction ϕ_0, deformation of an individual gel element can be measured by the displacement vector field $\boldsymbol{\xi}(\boldsymbol{x}, t)$. We can then write down a Cauchy strain tensor

$$\boldsymbol{e} = \frac{1}{2}\left[\boldsymbol{\nabla\xi} + (\boldsymbol{\nabla\xi})^{\mathrm{T}}\right] = \left[1 - \left(\frac{\phi}{\phi_0}\right)^{1/n}\right] \boldsymbol{I} + \boldsymbol{\epsilon}, \tag{2.1}$$

in n dimensions, separated into an isotropic part due to swelling and drying (changes in the local polymer fraction ϕ) and a traceless deviatoric part $\boldsymbol{\epsilon}$, which is assumed small. This also allows us to relate the divergence of the displacement field to ϕ, taking the trace of the strain tensor to find

$$\boldsymbol{\nabla}\cdot\boldsymbol{\xi} = n\left[1 - \left(\frac{\phi}{\phi_0}\right)^{1/n}\right]. \tag{2.2}$$

From this foundation, a constitutive relation for the Cauchy stress tensor can be deduced [14], describing the elastic and osmotic response in terms of two polymer-fraction-dependent material parameters: a shear modulus $\mu_s(\phi)$ and an osmotic pressure $\Pi(\phi)$. This shows how stresses on gel elements arises from pressures and deviatoric stresses,

$$\boldsymbol{\sigma} = -\left[p + \Pi(\phi)\right] \boldsymbol{I} + 2\mu_s(\phi)\boldsymbol{\epsilon}, \tag{2.3}$$

where p is the pervadic or pore pressure of the fluid component of the gel [17,18]. This pressure can be viewed physically as the pressure of the water in a gel that would be measured by a transducer separated from the bulk hydrogel by a permeable membrane, or it can be related to a chemical potential [17]. It is gradients in p that drive flow through a porous matrix, with Darcy's law setting the interstitial fluid flux $\boldsymbol{u} = -\left[k(\phi)/\mu_l\right]\boldsymbol{\nabla}p$, where $k(\phi)$ is the permeability and μ_l the fluid viscosity. It was shown in [14] that the polymer fraction evolves in time following the equation

$$\frac{\partial\phi}{\partial t} + \boldsymbol{q}\cdot\boldsymbol{\nabla}\phi + \boldsymbol{\nabla}\cdot\left[\frac{\phi k(\phi)}{\mu_l}\boldsymbol{\nabla}p\right] = 0 \quad \text{with} \quad \boldsymbol{q} = \boldsymbol{u} + \boldsymbol{u_p}. \tag{2.4}$$

The polymer velocity $\boldsymbol{u_p}$ can be approximated by $(\phi/\phi_0)^{-1/n}\,\partial\boldsymbol{\xi}/\partial t$ at leading order in the deviatoric strain [15], whilst the total flux vector $\boldsymbol{q}$ is solenoidal. This equation is coupled with Cauchy's momentum equation $\boldsymbol{\nabla}\cdot\boldsymbol{\sigma} = \boldsymbol{0}$ to close the system, relating gradients in p to those in ϕ and the deviatoric strain $\boldsymbol{\epsilon}$. Finally, the displacement field $\boldsymbol{\xi}$ is shown to satisfy a forced biharmonic equation

$$\nabla^4\boldsymbol{\xi} + n\boldsymbol{\nabla}\nabla^2\left(\frac{\phi}{\phi_0}\right)^{1/n} = \boldsymbol{0}, \tag{2.5}$$

with gradients in polymer fraction forcing the biharmonic operator of standard linear elasticity. Together, equations (2.2), (2.3), (2.4) and (2.5) allow us to describe the dynamics of a super-absorbent hydrogel and model the associated stresses, deformation and interstitial flows.

(a) The phase boundary

As discussed above, when gels are frozen at intermediate temperatures just below the equilibrium freezing temperature of water T_m, water is expelled from the gel to form pure ice outside of the pore structure, and so the phase boundary at the freezing front is between solid ice and partially-dried gel. The presence of pressures in the gel is known to modify the freezing temperature at this boundary. This effect arises from the (generalised) Clausius-Clapeyron relation [19] for the depression in freezing temperature to a liquidus temperature T_L,

$$\mathcal{L}\frac{T_L - T_m}{T_m} = \frac{\boldsymbol{n}\cdot\boldsymbol{\sigma}\cdot\boldsymbol{n} + p_0}{\rho_s} + \frac{p_l - p_0}{\rho_l}, \tag{2.6}$$

where ρ_s is the density of ice, ρ_l is the density of water, $\mathcal{L}$ is the specific latent heat of fusion, p_l is the fluid pressure and p_0 is a reference (atmospheric) pressure. As in [16], we assume that the ice is stress-free, and $\boldsymbol{n}\cdot\boldsymbol{\sigma}\cdot\boldsymbol{n} = -p_0$, so

$$\rho_l\mathcal{L}\frac{T_L - T_m}{T_m} = p_l - p_0 = p_l + \boldsymbol{n}\cdot\boldsymbol{\sigma}\cdot\boldsymbol{n}. \tag{2.7}$$

Since the work of Nye [20] on regelation, there has been much discussion on whether pressures or normal stresses ($\boldsymbol{n}\cdot\boldsymbol{\sigma}\cdot\boldsymbol{n}$) should be used on the right-hand side of this expression, a distinction that can make significant differences to the predictions where there are large overburden pressures or significant (deviatoric) elastic stresses. This question has recently been resolved by use of a careful derivation of the generalised Clapeyron equation in the presence of anisotropic stresses [19]. However, in our case, neither of these caveats apply, and the dominant influence on the right-hand side arises from concentration of the solvent and solute molecules, allowing us to model the freezing temperature depression as a purely colligative effect.

Therefore, following the same approach as the investigation of freezing colloidal suspensions in [21], we identify p_0 with P (the bulk pressure, equal to the sum of osmotic and pervadic pressures) and identify p_l with p. Therefore, the right-hand side is equal to $-\Pi(\phi)$, and the liquidus relation depends solely on osmotic pressures. Thus,

$$T_L = T_m\left(1 - \frac{\Pi(\phi)}{\rho_l\mathcal{L}}\right), \tag{2.8}$$

and the melting temperature of the ice is depressed by a quantity related to the local polymer volume fraction. Viewed as a boundary condition on the temperature field, this sets a lower freezing temperature at interfaces with drier gels, whilst viewed as a boundary condition on the hydrogel, this sets a polymer fraction greater than ϕ_0 at an undercooled interface. It is this latter interpretation that we will employ later when modelling cryosuction, finding that a value of $T < T_m$ at the ice–gel boundary drives drying of the gel and growth of the ice through interstitial flows towards this phase boundary.

The Stefan condition at the ice–gel boundary relates the growth of the ice layer to the difference in heat fluxes at the interface, via

$$\rho_s\mathcal{L}V_n = -\left[\mathcal{K}\left(\boldsymbol{n}\cdot\boldsymbol{\nabla}T\right)\right]_-^+, \tag{2.9}$$

where V_n is the rate of solidification normal to the freezing front, $\boldsymbol{n}$ is the unit normal pointing from the ice into the hydrogel, and $\mathcal{K}$ is the thermal conductivity, which may vary from phase to phase. The right-hand side is evaluated on either side of the boundary, with the $^+$ side taken to be in the gel and the $^-$ side in the ice in the present study.

In order for ice to grow, water must be supplied from the hydrogel, and therefore mass conservation implies

$$\rho_s V_n = -\rho_l\boldsymbol{u}\cdot\boldsymbol{n} \quad \text{so} \quad V_n + \frac{\rho_l}{\rho_s}\boldsymbol{u}\cdot\boldsymbol{n} = 0. \tag{2.10}$$

In other words, the mass of ice that grows must equal the mass of water expelled from the hydrogel. Since, as discussed above, $\rho_l/\rho_s \approx 1.1$ [13] and expansion in freezing is not the dominant effect driving damage, we henceforth assume $\rho_l/\rho_s = 1$ for simplicity, writing $\rho_s = \rho_l =$

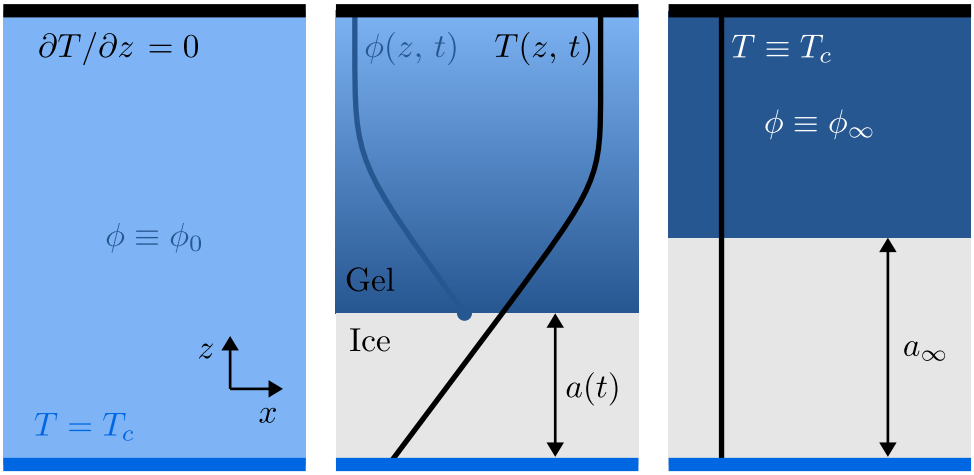

(a) The initial state (b) Ice forms in a layer (c) A steady state is reached

Figure 1: Schematic plots of the formation of ice in a box with infinite horizontal extent and a cooled lower boundary. Ice grows and the gel dries out but eventually a steady state is reached where the ice has thickness a_∞ and the gel is uniformly dried to a polymer fraction ϕ_∞.

ρ, though adapting our approach to account for volumetric expansion would be a straightforward extension. Using Darcy's law for the interstitial flux in the gel, it can be seen that pore pressure gradients are needed to drive ice growth,

$$\boldsymbol{u}\cdot\boldsymbol{n} = -\left[\frac{k(\phi)}{\mu_l}\left(\boldsymbol{n}\cdot\boldsymbol{\nabla}p\right)\right]^+ \quad \text{so} \quad \left[\frac{\rho\mathcal{L}k(\phi)}{\mu_l}\left(\boldsymbol{n}\cdot\boldsymbol{\nabla}p\right)\right]^+ = -\left[\mathcal{K}\left(\boldsymbol{n}\cdot\boldsymbol{\nabla}T\right)\right]^+_-. \tag{2.11}$$

This allows us to couple the pervadic pressure field in the gel with the temperature field, and model the cryosuction process whereby water is driven towards a freezing front. Provided the right-hand side of equation (2.11) is positive (i.e. there is freezing via equation (2.9)), $\boldsymbol{n}\cdot\boldsymbol{\nabla}p$ is positive in the gel, so pressure is higher in the bulk of the gel than at the interface, driving a flow towards the interface that allows the ice layer to grow.

3. Modelling unidirectional freezing

To begin our investigation into the freezing of gels, we consider a situation in which an initially uniformly-swollen layer of gel of infinite horizontal extent (in the x direction) is sandwiched between impermeable confining surfaces at $z = 0$ and $z = h$, as pictured in figure 1a. The upper surface is insulated, whilst the lower surface is cooled to a temperature $T_c < T_m$, so we expect ice to form here, occupying a layer of thickness $a(t)$ (figure 1b). We assume no variation in the horizontal direction, so all x derivatives are zero.

If the gel were fully contained within rigid boundaries in both the horizontal and vertical directions, arbitrarily large pressures would be generated through the expansion of water on change of phase, and ice would be unable to form, as the freezing temperature would be depressed by the high pressures [22]. In our model, water and gel are free to be displaced in the horizontal direction (parallel to x) but there is confinement in the vertical direction. Though this does generate a normal stress that acts throughout the gel, we have shown in equation (2.8) that the liquidus temperature relation is a purely colligative effect dependent only on osmotic pressures, since the deviatoric elastic stresses are small here. Hence, the presence of the fixed

upper boundary does not generate large elastic stresses that influence the growth of ice, and we safely continue to make the equal density assumption.

At the boundary between the ice and the gel, the temperature is equal to T_L, as defined by the liquidus relation of equation (2.8). We make the assumption that T_L is always greater than the ice-entry temperature of equation (1.1), and thus the ice that forms is pure, sited outside of the pores of the gel. In the ice layer, heat transfer is by conduction, whilst there is an advective component in the gel, giving the governing equations

$$\frac{\partial T}{\partial t} = \kappa_{\text{ice}} \frac{\partial^2 T}{\partial z^2} \quad \text{in } 0 \le z \le a(t), \tag{3.1a}$$

$$\frac{\partial T}{\partial t} + q_z \frac{\partial T}{\partial z} = \kappa_{\text{gel}} \frac{\partial^2 T}{\partial z^2} \quad \text{in } a(t) \le z \le h, \tag{3.1b}$$

where q_z is the vertical phase-averaged material flux and κ is the thermal diffusivity. These equations are solved subject to $T = T_c$ on $z = 0$ and $\partial T/\partial z = 0$ on $z = h$ (arising from the insulated boundary). The temperatures in each domain match at $z = a(t)$, with a value T_L, by definition.

Modelling the transport of heat through a porous medium such as a hydrogel is more complicated in reality than the simple advection-diffusion model presented here. A full model, based on thermoelasticity, takes into account contributions to the heat energy from deformation and from the entropic mixing of water and polymer molecules [23]. Even in regular non-deformable porous media, dispersion can be important owing to the tortuosity of pore-scale flows [24]. In the present study, we assume that all flows are slow and deformation occurs on sufficiently slow timescales that only advection and diffusion need to be considered. Furthermore, we make the assumption that diffusion of heat occurs in the gel with the diffusion coefficient κ_{gel} approximately equal to the thermal diffusivity of pure water. As a first model, this is justified on two counts: firstly, the gels remain highly swollen throughout, with $\phi_0 \sim 1 - 10\%$, and so the majority of a gel is formed of water, and secondly since the thermal diffusivities of the water and polymer components are similar in magnitude [25].

In this uniaxial configuration, take $n = 2$, and equation (2.4) describing the polymer fraction evolution becomes

$$\frac{\partial \phi}{\partial t} + q_z \frac{\partial \phi}{\partial z} + \frac{\partial}{\partial z}\left[\frac{\phi k(\phi)}{\mu_l}\frac{\partial p}{\partial z}\right] = 0 \quad \text{in } a(t) \le z \le h. \tag{3.2}$$

The solenoidal nature of the total flux vector $\boldsymbol{q}$ and horizontal uniformity together imply that q_z is a constant, since $\partial q_z/\partial z = 0$. However, since polymer and fluid velocities are zero on $z = h$, $q_z \equiv 0$ and there is no contribution from the advective term. Finally, Cauchy's momentum equation and the constitutive relation of equation (2.3) together give

$$\frac{\partial p}{\partial z} = -\frac{\partial \Pi}{\partial z} + \frac{\partial}{\partial z}\left[2\mu_s(\phi)\epsilon_{zz}\right]. \tag{3.3}$$

Since there is horizontal uniformity, we can deduce an expression for ϵ_{zz} in terms of ϕ. Uniformity implies that $e_{xx} = 0$ – i.e. that there is no strain parallel to the ice–gel interface. Thus, using equation (2.1), $\epsilon_{xx} = (\phi/\phi_0)^{1/2} - 1$, and $\epsilon_{zz} = -\epsilon_{xx}$ by the traceless nature of $\boldsymbol{\epsilon}$. We can then substitute this expression into equation (3.3) to show that $\partial p/\partial z \propto \partial \phi/\partial z$, through

$$\frac{\partial p}{\partial z} = -\frac{\mu_l D(\phi)}{\phi k(\phi)}\frac{\partial \phi}{\partial z} \quad \text{with} \quad D(\phi) = \frac{\phi k(\phi)}{\mu_l}\left\{\frac{\partial \Pi}{\partial \phi} + 2\frac{\partial}{\partial \phi}\left[\mu_s(\phi)\left(\phi/\phi_0\right)^{1/2}\right]\right\}, \tag{3.4}$$

where $D(\phi)$ can be viewed as a nonlinear polymer diffusivity. This allows us to write the governing equations solely in terms of ϕ and T,

$$\frac{\partial T}{\partial t} = \kappa_{\text{gel}} \frac{\partial^2 T}{\partial z^2} \quad \text{in } a(t) \le z \le h, \tag{3.5a}$$

$$\frac{\partial \phi}{\partial t} = \frac{\partial}{\partial z}\left[D(\phi) \frac{\partial \phi}{\partial z} \right] \quad \text{in } a(t) \le z \le h, \tag{3.5b}$$

$$\frac{\partial T}{\partial t} = \kappa_{\text{ice}} \frac{\partial^2 T}{\partial z^2} \quad \text{in } 0 \le z \le a(t). \tag{3.5c}$$

The boundary conditions on $T(z,\, t)$ and $\phi(z,\, t)$ are

$$T(0,\, t) = T_c, \quad T(a(t),\, t) = T_L, \quad \left.\frac{\partial T}{\partial z}\right|_{z=h} = 0 \quad \text{and} \tag{3.6a}$$

$$\left.\frac{\partial \phi}{\partial z}\right|_{z=h} = 0, \quad \left.\frac{\partial \phi}{\partial z}\right|_{z=a(t)} = \frac{\phi}{\rho \mathcal{L} D(\phi)} \left[\mathcal{K} \frac{\partial T}{\partial z} \right]_{z=a(t)^-}^{z=a(t)^+}, \tag{3.6b}$$

respectively. The first condition on $\partial\phi/\partial z$ arises from combining equation (3.4) with no flow through the top boundary, and the second arises from equation (2.11). Growth of the ice layer $0 \le z \le a(t)$ is governed by the Stefan condition of equation (2.9),

$$\rho \mathcal{L} \frac{\mathrm{d}a}{\mathrm{d}t} = -\left[\mathcal{K} \frac{\partial T}{\partial z} \right]_{z=a(t)^-}^{z=a(t)^+}. \tag{3.7}$$

This system of equations (3.5)–(3.7) is the same as that found in [21] for the freezing of colloidal suspensions, albeit with a different compositional diffusivity that is modified by deviatoric stresses. This is to be expected, since it is only through elastic stresses (arising from cross-linking of the polymer scaffold) that our physical situation differs from a colloid.

(a) Steady state

Recent experiments freezing hydrogels in a rigid container with a loose upper surface show that a steady state is reached where ice has formed with a uniform temperature T_c throughout. Since we are neglecting thermal expansion in the present model, we ignore the movement of this upper surface and assume that the container height remains equal to h throughout. Ice formation draws water from the surrounding gel, raising the osmotic pressure such that the liquidus temperature eventually reaches T_c and no further freezing can occur. This leaves behind a uniformly-dried gel and a layer of pure ice [1], as pictured in figure 1c. We start by seeking a steady state of the governing equations (3.5), and find that the only admissible temperature field is $T \equiv T_c$ in $0 \le z \le h$. Thus, as seen in the experiments, $T_L = T_c$ in this state. Equation (3.5*b*) for ϕ shows that the only steady state solution has a uniform polymer fraction ϕ_∞, and we can use the liquidus relation (2.8) to show that

$$T_c = T_m \left[1 - \frac{\Pi(\phi_\infty)}{\rho \mathcal{L}} \right], \tag{3.8}$$

implicitly determining ϕ_∞ in terms of the undercooling and the material properties. By conservation of polymer, we can also deduce the steady-state ice thickness a_∞,

$$h\phi_0 = (h - a_\infty)\phi_\infty \quad \text{so} \quad a_\infty = h\left(1 - \frac{\phi_0}{\phi_\infty}\right). \tag{3.9}$$

This allows us to deduce the value of the osmotic pressure purely in terms of measurable quantities a_∞ and T_c, and can vary the value of T_c to deduce a constitutive relation for $\Pi(\phi)$.

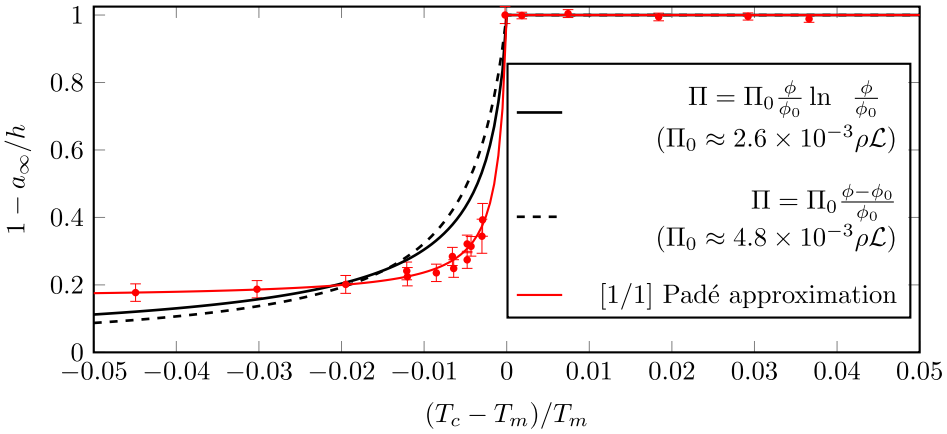

Figure 2: Plots of the steady-state gel thickness against base temperature for different degrees of undercooling. The red points are the experimental results from [1], showing no ice formation at $T_c = T_m = 0\,^\circ\mathrm{C}$, and then a thicker ice layer as the temperature is lowered. The two black lines show the predicted ice thicknesses of equation (3.9) for linear and logarithmic osmotic pressures in our model, with the fit parameter Π_0 deduced from a nonlinear least-squares fitting to the experimental data using Matlab's `lsqnonlin`. The red curve shows the best fit Padé approximant form for Π (3.11) from the experimental data.

Specifically,

$$\Pi\left(\frac{1}{1 - a_\infty/h}\right) = \rho\mathcal{L}\frac{T_m - T_c}{T_m}. \tag{3.10}$$

Figure 2 shows how this steady ice layer thickness can be seen to depend on the specific form of the constitutive relation for $\Pi(\phi)$. The dashed curve shows a linear osmotic pressure, of the form that we will use in the present study, whilst the solid curve shows the logarithmic osmotic pressure in a Hencky effective elastic model [26]. We can use the results from experiments to deduce a fitted form of the osmotic pressure function, as shown in the red curve of figure 2. Assuming that Π takes the form of a $[1/1]$ Padé approximant with $\Pi(\phi_0) = 0$, we fit parameters to find the other constants. In the case of the experimental results in [1],

$$\Pi(\phi) \approx \frac{1 \times 10^{-3}\rho\mathcal{L}}{\phi_0}\frac{\phi - \phi_0}{1 - \phi/(6.6\phi_0)}. \tag{3.11}$$

This shows that the osmotic pressure has a zero at ϕ_0, as would be expected, but also that $\Pi \to \infty$ as $\phi \to 6.6\phi_0$, introducing an upper (dried) limit for the polymer fraction, evident in the plateau of figure 2, where $1 - a_\infty/h \approx 1/6.6$.

Qualitatively, our model's theoretical predictions in figure 2 match the experimental measurements made by [1], with the ice layer thickness approaching zero as $T \to T_m$ from below. However, a linear or logarithmic osmotic pressure does not reproduce the plateau apparent from experiments, where the gel can be neither dried nor compressed any further, at $1 - a_\infty/h \approx 0.2$ in this case, and all that remains of the hydrogel is a polymer scaffold. Since our model is only valid for small deviatoric strains in the linear regime, we continue to use a linear osmotic pressure since we are unlikely to reach such a plateau, where there is extreme drying and therefore large strain.

(b) Non-dimensionalisation and linearisation

In order to model the transient evolution of the ice layer, we return to the governing equations (3.5) and boundary conditions (3.6). We now make the assumption that the material properties k

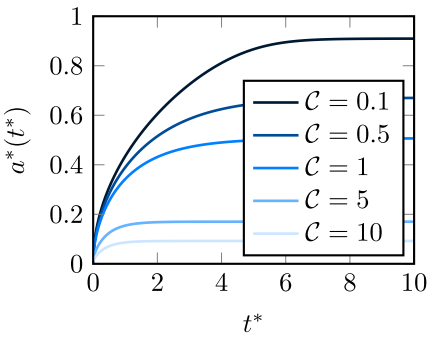

(a) Plots of ice thickness against time

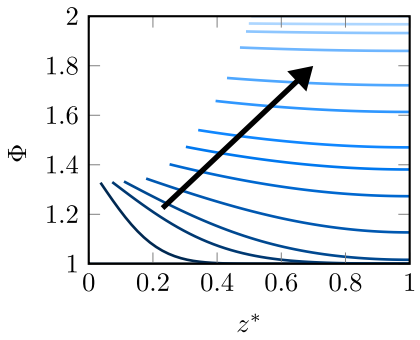

(b) Plots of the polymer fraction field at different times when $\mathcal{C} = 1$

Figure 3: Numerical solutions to equations (3.15) with the temperature field of (3.16) showing the growth of the ice layer and the subsequent drying of the gel. In all cases, $Le/\mathcal{S} = 0.1$.

and μ_s do not depend on polymer fraction ϕ and assume a linear osmotic pressure

$$\Pi(\phi) = \Pi_0 \frac{\phi - \phi_0}{\phi_0}. \tag{3.12}$$

These assumptions, alongside the approximation that $\phi \approx \phi_0$ throughout the drying process, allow us to work in the limit of a constant compositional diffusivity $D(\phi) = D$, and we can non-dimensionalise the governing equations (3.5) through the introduction of new variables

$$z^* = \frac{z}{h}; \quad a^* = \frac{a(t)}{h}; \quad t^* = \frac{Dt}{h^2}; \quad \theta = \frac{T - T_c}{T_m - T_c}; \quad \Phi = \frac{\phi}{\phi_0}, \tag{3.13}$$

with

$$D = \frac{k}{\mu_l}\left(\Pi_0 + \mu_s\right), \tag{3.14}$$

from equation (3.4). Then, the system of equations and boundary conditions driving ice growth are

$$\frac{\partial \theta}{\partial t^*} = Le_{\text{gel}} \frac{\partial^2 \theta}{\partial z^{*2}} \quad \text{in } a^*(t^*) \le z^* \le 1, \tag{3.15a}$$

$$\frac{\partial \Phi}{\partial t^*} = \frac{\partial^2 \Phi}{\partial z^{*2}} \quad \text{in } a^*(t^*) \le z^* \le 1, \tag{3.15b}$$

$$\frac{\partial \theta}{\partial t^*} = Le_{\text{ice}} \frac{\partial^2 \theta}{\partial z^{*2}} \quad \text{in } 0 \le z^* \le a^*(t^*), \tag{3.15c}$$

$$\frac{\mathrm{d}a^*}{\mathrm{d}t^*} = -\left[\frac{Le}{\mathcal{S}} \frac{\partial \theta}{\partial z^*}\right]_{z^* = a^*(t^*)^-}^{z^* = a^*(t^*)^+}, \tag{3.15d}$$

$$\theta(0,\, t^*) = 0,\ \theta(a^*(t^*), t^*) = 1 - \mathcal{C}\left[\Phi(a^*(t^*),\, t^*) - 1\right],\ \left.\frac{\partial \theta}{\partial z^*}\right|_{z^*=1} = 0 \quad \text{and} \tag{3.15e}$$

$$\left.\frac{\partial \Phi}{\partial z^*}\right|_{z^*=1} = 0, \quad \left.\frac{\partial \Phi}{\partial z^*}\right|_{z^* = a^*(t^*)} = \left[\frac{Le}{\mathcal{S}} \frac{\partial \theta}{\partial z^*}\right]_{z^* = a^*(t^*)^-}^{z^* = a^*(t^*)^+}. \tag{3.15f}$$

where $Le = \kappa/D$ is the Lewis number, representing the ratio of thermal to compositional diffusivities, and $\mathcal{S} = \mathcal{L}/c_p(T_m - T_c)$ is the Stefan number. $\mathcal{C} = \Pi_0 T_m/\rho\mathcal{L}(T_m - T_c)$ is a dimensionless parameter representing the importance of osmotic effects relative to the latent heat of fusion, quantifying the degree of undercooling due to osmotic pressure at the phase boundary.

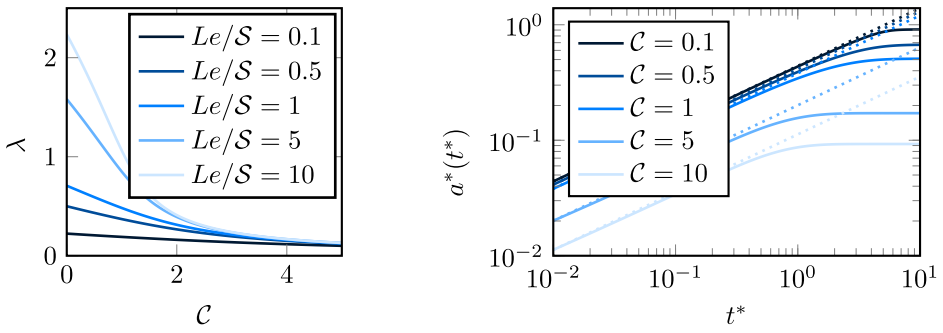

(a) Plots of the growth rate λ against undercooling amount $\mathcal{C}$

(b) Comparisons with the full finite-domain solution (similarity solution for $a^*(t^*)$ shown as dotted lines). Here, $Le/\mathcal{S} = 0.1$ and both scales are logarithmic.

Figure 4: Plots of the growth rate λ of the early-time similarity solution and a comparison of the early-time solution for $a^*(t^*)$ with full numerical results, showing close agreement until the layer thickness is appreciable compared with the container height.

We treat the thermal properties of the hydrogel as approximately the same as those of pure liquid water since the polymer fraction of such gels can be very small [25,27]. Thus, $Le_{\text{gel}} = Le_{\text{water}}$ and $\mathcal{S}_{\text{gel}} = \mathcal{S}_{\text{water}}$. Thermal diffusivities of water and ice are of the order 10^{-7} to $10^{-6}\,\text{m}^2\text{s}^{-1}$, yet the poroelastic diffusivity of hydrogels, D, scales like $k\Pi_0/\mu_l$, approximately of the order 10^{-9} to $10^{-8}\,\text{m}^2\text{s}^{-1}$ using values from the literature [28,29]. Hence, it is clear that heat diffuses through the system much more rapidly than water through the pore spaces. This motivates considering the limit $Le \gg 1$, implying a linear temperature field in the ice and a uniform temperature field in the gel

$$\theta = \begin{cases} \left\{1 - \mathcal{C}\left[\Phi(a^*(t^*), t^*) - 1\right]\right\} \dfrac{z^*}{a^*(t^*)} & \text{in } 0 \le z^* \le a^*(t^*) \\ 1 - \mathcal{C}\left[\Phi(a^*(t^*), t^*) - 1\right] & \text{in } a^*(t^*) \le z^* \le 1 \end{cases}, \tag{3.16}$$

or, physically, that the gel has a uniform temperature equal to the liquidus temperature at the phase boundary and the heat fluxes in the ice are vertically uniform.

Numerical solutions are plotted in figure 3 showing the growth of the ice layer and the evolution of the polymer fraction field, showing how the gel dries out from the phase boundary inwards, with the ice thickness increasing. In all cases, there is an approach to the steady state computed in equation (3.8) in which

$$\Phi_\infty = 1 + \frac{1}{\mathcal{C}} \quad \text{thus} \quad a^*_\infty = \frac{\mathcal{C}}{1+\mathcal{C}}. \tag{3.17}$$

(c) Early-time ice growth

At early times, the ice growth boundary condition shows that there is rapid growth, with the condition of equation (3.15*d*) becoming

$$\frac{\mathrm{d}a^*}{\mathrm{d}t^*} = \frac{Le_{\text{ice}}}{\mathcal{S}_{\text{ice}}} \frac{1 - \mathcal{C}\left[\Phi(a^*(t^*), t^*) - 1\right]}{a^*(t^*)}, \tag{3.18}$$

under the assumption of a linear temperature profile in the ice and a uniform temperature (equal to the liquidus temperature) in the gel. This shows that the ice layer has an infinite growth rate at $t^* = 0$, and thus the early time behaviour may not be well-resolved by numerical modelling. At

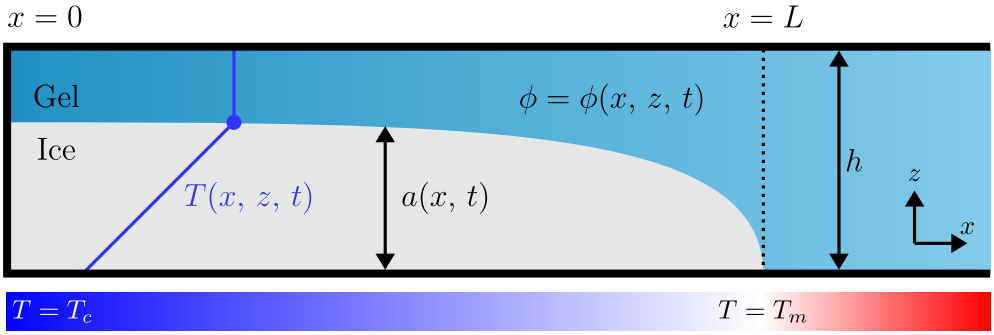

Figure 5: A diagram illustrating the physical setup for this problem, with a gel sandwiched between an insulating upper plate at $z = h$, an impermeable wall at $z = 0$ and a cooled lower plate at $z = 0$ with a temperature gradient. An ice lens forms in the region $0 \leq x \leq L$ with thickness $a(x, t)$.

these early times, however, the gel drying is confined to a thin boundary layer close to $z^* = a^*(t^*)$, so we model the gel domain as effectively infinite in extent, ignoring any effects of the lid at $z^* = 1$.

In this domain, a similarity solution to the governing equations exists, taking the similarity variable $\chi = z^*/2\sqrt{t^*}$ and letting $a^*(t^*) = 2\lambda\sqrt{t^*}$. The resultant equations are solved by

$$\Phi = 1 + \frac{Le}{\mathcal{S}} \frac{\operatorname{erfc} \chi}{\frac{2\lambda}{\sqrt{\pi}} e^{-\lambda^2} + \frac{\mathcal{C}Le}{\mathcal{S}} \operatorname{erfc} \lambda}, \tag{3.19}$$

where the Lewis and Stefan numbers are those for ice, and λ satisfies

$$\frac{Le}{\mathcal{S}} \left(1 - \sqrt{\pi}\mathcal{C}\lambda e^{\lambda^2} \operatorname{erfc} \lambda\right) = 2\lambda^2. \tag{3.20}$$

Figure 4a shows the dependence of λ on the two non-dimensional parameters in this problem, $Le/\mathcal{S}$ and $\mathcal{C}$. It is seen that increasing $\mathcal{C}$ leads to slower ice growth, and that increasing $Le/\mathcal{S}$ has the opposite effect. This can be understood by noticing that a larger value of $\mathcal{C}$ imposes a lower liquidus temperature at the phase boundary, and thus the magnitude of $\partial\theta/\partial z^*$ is reduced, such that thermal fluxes are smaller and ice growth is retarded. Taking a larger Lewis number relative to the Stefan number, however, suggests faster thermal diffusion or a cooler lower boundary, so leads to faster freezing.

Figure 4b illustrates how the similarity solution's predictions for $a^*(t^*)$ compare with the full numerical solutions, showing close agreement as $t^* \to 0$, with a divergence as time increases and the ice grows. Eventually, the effect of the finite domain becomes marked when the gel dries and is compressed, and there is a lack of water to supply to the growing frozen layer.

4. Ice lens formation with temperature gradients

In the modelling of the previous section, advective effects in the polymer fraction evolution equation can be neglected, and the freezing process leads to cryosuction in one direction, from more swollen gel closer to the top boundary towards the phase boundary. As a result, only vertical stresses form in the gel as it is displaced in a horizontally-uniform manner. In order to understand the processes by which porous media may be damaged by cryosuction, recent experiments have replaced the uniformly cooled lower boundary of section 3 by a boundary with a temperature gradient, with more ice forming in cooler sections and no ice forming along the boundary where $T > T_m$ [1]. Such a situation is pictured in figure 5, where the lower boundary is cooled to a

temperature

$$T = \begin{cases} T_m - \frac{1}{2}(T_m - T_c)\left(1 + \cos\frac{\pi x}{L}\right) & x \le L \\ T_m & x > L \end{cases} \tag{4.1}$$

where the temperature variation occurs over a lengthscale L, and $\partial T/\partial x = 0$ at $x = 0$ and $x = L$ (we have chosen the simple form of equation (4.1) to have continuous temperatures and heat fluxes, even at the solid boundary $x = 0$ and at the point $x = L$ where $T = T_m$). The effect of this cooling is to produce ice occupying the region $0 \le z \le a(x, t)$, with the space above the ice layer comprising unfrozen hydrogel. Since the ice growth occurs in a tapered manner, with a sharp nose at the freezing front, it is natural to draw parallels with the propagation of cracks in elastic materials, since the formation of an ice lens looks qualitatively like the growth of a crack.

In Irwin's classical study of fracture mechanics [30], it is shown that cracks can propagate through materials in three distinct ways, called mode-I, mode-II and mode-III. Mode-I cracks involve normal stresses at the crack tip 'pushing' the material outwards, perpendicular to the direction of the crack, as the fracture grows. In mode-II cracks, shear stresses parallel to the direction of the crack (but perpendicular to the crack front in three dimensions) dominate the opening, so that material 'slides' out of the way. Finally, mode-III cracks involve a shear stress acting parallel to the crack tip but along the plane of the crack front, tearing apart either side. Since our study is two-dimensional, mode-III cracks cannot be seen. In this section, we apply our freezing model to the growth of ice lenses, and seek to explain the observation that the form of the cryoscution-driven stresses in the hydrogel are heavily dependent on mechanical boundary conditions on the displacement field [1], with lens formation akin to a mode-II crack when the gel is adhered to the walls, and akin to a mode-I crack when it is free to slide.

In classical fracture mechanics, the adhesion strength is important in setting both the shape of a crack as it forms and the dynamics of its formation [31], and in our case the hydrogel must be pulled away from the lower boundary for the ice lens to form. Experimentally, it is seen that the shape of the ice lens that forms is largely independent of adhesion strength [1], with different silane treatments on the glass surface showing qualitatively equivalent results. Furthermore, once an ice lens has formed on the lower surface $0 \le x \le L$, there is no growth of the crack horizontally, and since the crack does not propagate, none of the dynamics of lens formation from $t = 0$ onwards depend on the adhesion strength, unlike when a crack grows parallel to its tip through a material that is fracturing. Therefore, in the present study, we neglect the effect of adhesion strength on the formation of ice lenses, but remark that significant stresses near the lens tip may lead to detachment of the gel from the boundary in front of $x = L$. This could affect the stress and strain fields in the region of the lens tip, dependent on the adhesive strength, and therefore the shape of the ice lens and nature of stresses in the gel near this point cannot be fully determined without incorporation of adhesive effects. In this paper, we will therefore restrict our attention to the shape of the lens away from the lens tip, and consider only stresses in the bulk of the hydrogel.

Again making the large Lewis number limit of section 3, we assume that the temperature in $a(x, t) \le z \le h$ is independent of z, equal to its value on the phase boundary $z = a(x, t)$, and that within the ice the temperature varies linearly with depth

$$T = T_m - \frac{1}{2}(T_m - T_c)\left(1 + \cos\frac{\pi x}{L}\right) + \left[T_L(x, t) - T_m + \frac{1}{2}(T_m - T_c)\left(1 + \cos\frac{\pi x}{L}\right)\right]\frac{z}{a}, \tag{4.2}$$

where $T_L(x, t)$ is the interfacial liquidus temperature on $z = a(x, t)$, which is a function of the local polymer fraction. The equations describing the gel dynamics are

$$\frac{\partial \phi}{\partial t} + \boldsymbol{q} \cdot \boldsymbol{\nabla}\phi + \boldsymbol{\nabla} \cdot \left[\frac{\phi k(\phi)}{\mu_l}\boldsymbol{\nabla} p\right] = 0 \quad \text{in } a(x, t) \le z \le h, \tag{4.3a}$$

$$\boldsymbol{\nabla} p + \boldsymbol{\nabla} \Pi = 2\boldsymbol{\nabla} \cdot [\mu_s(\phi)\boldsymbol{\epsilon}] \quad \text{in } a(x, t) \le z \le h, \tag{4.3b}$$

with equation (4.3*b*) arising from Cauchy's momentum equation combined with the constitutive relation (2.3). Finally, the Stefan condition (2.9) for the interfacial evolution implies

$$\rho\mathcal{L}\frac{\mathrm{d}a}{\mathrm{d}t} = \mathcal{K}_{\mathrm{ice}}\left[\frac{\partial T}{\partial z} - \frac{\partial a}{\partial x}\frac{\partial T}{\partial x}\right]_{z=a(x,\,t)^-}. \tag{4.4}$$

Again we assume that the permeability and shear modulus are both constants, and that the osmotic pressure is a linear function of ϕ, in the form of equation (3.12). Let $\Phi = \phi/\phi_0$, and use the result that $2\boldsymbol{\nabla}\cdot\boldsymbol{\epsilon} = \nabla^2\boldsymbol{\xi}$ in two dimensions [26] to express equation (4.3*a*) as

$$\frac{\partial\Phi}{\partial t} + \Phi^{-1/2}\frac{\partial\boldsymbol{\xi}}{\partial t}\cdot\boldsymbol{\nabla}\Phi + \frac{k}{\mu_l}\Phi\nabla^2 p = 0 \quad \text{so} \tag{4.5}$$

$$\frac{\partial\Phi}{\partial t} + \Phi^{-1/2}\frac{\partial\boldsymbol{\xi}}{\partial t}\cdot\boldsymbol{\nabla}\Phi = \frac{k\Pi_0}{\mu_l}\left(\Phi + \mathcal{M}\Phi^{1/2}\right)\nabla^2\Phi, \tag{4.6}$$

using the expression for $\boldsymbol{q}$ in equation (2.4) and rewriting $\boldsymbol{\nabla}\cdot\boldsymbol{\xi}$ with equation (2.2). The shear parameter $\mathcal{M} = \mu_s/\Pi_0$ represents the importance of shear stresses relative to osmotic pressures.

Seeking semi-analytical solutions to this problem, we restrict our attention to situations where the thickness of the channel is much less than the lengthscale over which the temperature varies (i.e. $\varepsilon = h/L \ll 1$). Scaling the terms in equation (4.6), where the two-dimensional displacement vector field $\boldsymbol{\xi}$ has horizontal component ξ and vertical component η,

$$x^* = \frac{x}{L};\ z^* = \frac{z}{h};\ \xi^* = \frac{\xi}{L};\ \eta^* = \frac{\eta}{L};\ a^* = \frac{a(x,\,t)}{h};\ \Phi = \frac{\phi}{\phi_0}, \tag{4.7}$$

it becomes clear that the leading-order contributions to fluid transport occur on the vertical diffusive timescale $\mu_l h^2/k\Pi_0$, and so equation (4.6) becomes

$$\frac{\partial\Phi}{\partial t^*} + \Phi^{-1/2}\frac{\partial\xi^*}{\partial t^*}\frac{\partial\Phi}{\partial x^*} + \Phi^{-1/2}\frac{\partial\eta^*}{\partial t^*}\frac{\partial\Phi}{\partial z^*} = \left(1 + \mathcal{M}\Phi^{-1/2}\right)\frac{\partial^2\Phi}{\partial z^{*2}}, \tag{4.8}$$

at leading order in ε, with t^* a dimensionless time scaled with the vertical diffusive timescale. All further contributions to the diffusive term on the right-hand side occur at order ε^2.

(a) Flow boundary conditions and ice growth

At the phase boundary, equation (4.4) prescribes the rate of ice growth, which non-dimensionalises using the variables of the section above to give

$$\frac{\mathrm{d}a^*}{\mathrm{d}t^*} = \frac{Le}{\mathcal{S}}\frac{\frac{1}{2}\left(1 + \cos\pi x^*\right) - \mathcal{C}(\Phi - 1)}{a^*}, \tag{4.9}$$

where $\mathcal{S}$ and $\mathcal{C}$ are the Stefan and undercooling numbers respectively, as defined above, and $Le = \kappa/D$ represents the ratio between thermal and compositional diffusivities, where $D = k\Pi_0/\mu_l$.

There are also boundary conditions on the interstitial flow field, with no flow through the upper boundary $z^* = 1$ or the wall at $x^* = 0$. Similarly, we expect $\partial p^*/\partial x^* = 0$ as $x^* \to \infty$, representing no flow far from the freezing front. Scaling pressures with Π_0, equation (4.3*b*) implies that

$$\frac{\partial p^*}{\partial x^*} = -\frac{\partial\Phi}{\partial x^*} + \mathcal{M}\left(\frac{\partial^2\xi^*}{\partial x^{*2}} + \varepsilon^{-2}\frac{\partial^2\xi^*}{\partial z^{*2}}\right) \quad \text{and} \quad \frac{\partial p^*}{\partial z^*} = -\frac{\partial\Phi}{\partial z^*} + \mathcal{M}\left(\varepsilon^2\frac{\partial^2\eta^*}{\partial x^{*2}} + \frac{\partial^2\eta^*}{\partial z^{*2}}\right), \tag{4.10}$$

giving the boundary conditions

$$\frac{\partial\Phi}{\partial x^*} = \mathcal{M}\frac{\partial^2\xi^*}{\partial x^{*2}} \quad \text{on } x^* = 0,\ x^* \to \infty \quad \text{and} \quad \frac{\partial\Phi}{\partial z^*} = \mathcal{M}\frac{\partial^2\eta^*}{\partial z^{*2}} \quad \text{on } z^* = 1. \tag{4.11}$$

In fact, symmetry arguments allow us to assume $\partial\Phi/\partial x^* = 0$ on both $x^* = 0$ and as $x^* \to \infty$, setting stronger conditions on the polymer fraction field. Finally, cryosuction sets a boundary condition on $\partial p^*/\partial z^*$ on the phase boundary, since the rate of water supplied to the ice must match the rate of ice growth. Making the same assumptions of equal densities as before, with

slenderness allowing us to assume that the normal fluid velocity at the ice–gel boundary is vertical,

$$\mathcal{M}\frac{\partial^2 \eta^*}{\partial z^{*2}} - \frac{\partial \Phi}{\partial z^*} = \frac{\mathrm{d}a^*}{\mathrm{d}t^*} \quad \text{on } z^* = a^*(t^*). \tag{4.12}$$

Provided that we can find expressions for the displacement field in terms of the polymer fraction Φ, equation (4.8), the growth condition (4.9), and boundary conditions (4.11) and (4.12) describe the formation of ice lenses fully.

(b) Displacement field

In order to balance vertical deviatoric stresses with horizontal bulk pressure gradients, pressure must scale like ε^{-2}, with $\mathcal{P} = \varepsilon^2(p^* + \Phi - 1)$. Hence, the vertical component of Cauchy's momentum equation implies that $\partial\mathcal{P}/\partial z^* = 0$ at leading order, so

$$\xi^* = \frac{1}{2\mathcal{M}}\frac{\partial \mathcal{P}}{\partial x^*} z^{*2} + A(x^*)z^* + B(x^*). \tag{4.13}$$

Hence,

$$\eta^* = 2\int_{z^*}^{1} \Phi^{1/2}\,\mathrm{d}z' + \frac{1}{6\mathcal{M}}\frac{\partial^2 \mathcal{P}}{\partial x^{*2}}\left(1 - z^{*3}\right) + \frac{1}{2}\frac{\partial A}{\partial x^*}\left(1 - z^{*2}\right) + \left(\frac{\partial B}{\partial x^*} - 2\right)(1 - z^*), \tag{4.14}$$

using equation (2.2) and the fact that $\eta^* = 0$ on $z^* = 1$. Since $\xi^* = 0$ on $x^* = 0$, it is clear that $A(0) = B(0) = \partial\mathcal{P}/\partial x^* = 0$ here. Recent experiments detailed in [1] compare the effect of two boundary conditions at the point where the gel meets the top boundary of the container. To find the form of A, B and $\partial\mathcal{P}/\partial x^*$, we must impose either free-slip or no-slip boundary conditions at the walls and ice–gel boundary.

(i) No-slip boundary conditions

In the case where $\xi^* = 0$ on both $z^* = 1$ and $z^* = a^*(x^*)$, we expect a parabolic profile for the horizontal displacement,

$$\xi^*_{\mathrm{NS}} = -\frac{1}{2\mathcal{M}}\frac{\partial \mathcal{P}}{\partial x^*}\left(1 - z^*\right)\left(z^* - a^*\right), \tag{4.15a}$$

with

$$\eta^*_{\mathrm{NS}} = 2\int_{z^*}^{1}\left(\Phi^{1/2} - 1\right)\mathrm{d}z' - \frac{(1 - z^*)^2}{12\mathcal{M}}\left[\frac{\partial^2 \mathcal{P}}{\partial x^{*2}}\left(1 + 2z^* - 3a^*\right) - 3\frac{\partial a^*}{\partial x^*}\frac{\partial \mathcal{P}}{\partial x^*}\right]. \tag{4.15b}$$

On $z^* = a^*(x^*)$, it is also apparent that the vertical displacement must be equal to a^* – points that start out on the lower boundary must remain on this lower boundary – resulting in a first-order ordinary differential equation for $\partial\mathcal{P}/\partial x^*$ from setting $z^* = a^*$ in equation (4.15*b*). Since $\partial\mathcal{P}/\partial x^* = 0$ at $x^* = 0$, this can be solved for the horizontal pressure gradient, fully specifying the form of the displacement field. Specifically,

$$\frac{\partial^2 \mathcal{P}}{\partial x^{*2}} - \frac{3}{1 - a^*}\frac{\partial a^*}{\partial x^*}\frac{\partial \mathcal{P}}{\partial x^*} - \frac{24\mathcal{M}}{(1 - a^*)^3}\int_{a^*}^{1}\left(\Phi^{\frac{1}{2}} - 1\right)\mathrm{d}z' + \frac{12\mathcal{M}a^*}{(1 - a^*)^3} = 0. \tag{4.16}$$

For the assumptions of LENS modelling to hold, we require the deviatoric strains to be small. Using the definitions

$$\epsilon_{zz} = \frac{\partial \eta^*}{\partial z^*} - 1 + \Phi^{1/2} \quad \text{and} \quad \epsilon_{xz} = \frac{1}{2}\left[\frac{1}{\varepsilon}\frac{\partial \xi^*}{\partial z^*} + \varepsilon\frac{\partial \eta^*}{\partial x^*}\right], \tag{4.17}$$

these conditions reduce to requiring

$$1 - \Phi^{1/2} + \frac{1 - z^*}{2\mathcal{M}}\left[(z^* - a^*)\frac{\partial^2 \mathcal{P}}{\partial x^{*2}} - \frac{\partial a^*}{\partial x^*}\frac{\partial \mathcal{P}}{\partial x^*}\right] \ll 1 \quad \text{and} \quad \frac{2z^* - (1 + a^*)}{2\mathcal{M}}\frac{\partial \mathcal{P}}{\partial x^*} \ll 1. \tag{4.18}$$

These conditions can both be satisfied in the limit $\mathcal{M} \gg 1$ and $\mathcal{C} \gg 1$, where the gel is stiff and there is limited drying ($\Phi \approx 1$), since large $\mathcal{C}$ ensures that little drying must occur to lower the liquidus

temperature to below the lower boundary cooled temperature. Notice that the requirement that $\mathcal{M} \gg 1$ implies that horizontal displacements ξ^*_{NS} must be small in magnitude.

(ii) Free-slip boundary conditions

If we instead allow the gel to slip along the top boundary and phase boundary, but instead impose the requirement that the shear strain ϵ_{xz} is zero on the boundaries, we require $\partial \xi^*/\partial z^* = 0$ on both $z^* = a^*$ and $z^* = 1$ at leading order in the aspect ratio. This enforces $\partial \mathcal{P}/\partial x^* = 0$, with little flow in the horizontal direction, and shows that the gel deforms by stretching horizontally like a block. In this case,

$$\xi^*_{\mathrm{FS}} = B(x^*) \quad \text{and} \quad \eta^*_{\mathrm{FS}} = 2\int_{z^*}^{1} \left(\Phi^{1/2} - 1\right) \mathrm{d}z' + \frac{\partial B}{\partial x^*}\left(1 - z^*\right). \tag{4.19}$$

Again requiring $\eta^* = a^*$ when $z^* = a^*$ sets the value of the final parameter, $B(x^*)$, such that

$$\xi^*_{\mathrm{FS}} = \int_0^{x^*} \left[\frac{a^*}{1-a^*} - \frac{2}{1-a^*}\int_{a^*}^{1} \left(\Phi^{1/2} - 1\right) \mathrm{d}z'\right] \mathrm{d}x', \tag{4.20a}$$

$$\eta^*_{\mathrm{FS}} = 2\int_{z^*}^{1} \left(\Phi^{1/2} - 1\right) \mathrm{d}z' + \frac{1-z^*}{1-a^*}\left[a^* - 2\int_{a^*}^{1} \left(\Phi^{1/2} - 1\right) \mathrm{d}z'\right]. \tag{4.20b}$$

Notice that there is no dependence on the stiffness of the gel in the displacement field, since the parameter $\mathcal{M}$ does not appear. This only affects the rate at which deswelling occurs, but since the material is not anchored at its boundaries, the intrinsic stiffness is unimportant. Unlike in the no-slip case, we are guaranteed that shear strains are small everywhere in this case, since $\partial \xi^*/\partial z^* = 0$ and the gel is stretched plug-like in the horizontal direction. For normal deviatoric strains to be small, we require

$$1 - \Phi^{1/2} - \frac{a^*}{1-a^*} + \frac{2}{1-a^*}\int_{a^*}^{1} \left(\Phi^{1/2} - 1\right) \mathrm{d}z' \ll 1, \tag{4.21}$$

which again can only be satisfied if $\Phi \approx 1$ and a^* is small, which occurs when $\mathcal{C}$ is large, a superset of the parameter range where LENS theory is valid in the no-slip case. The absence of pinned boundaries prevents large deviatoric strains from building as easily as in the case of no-slip boundaries, resulting in weaker constraints on the gel for model validity, and allowing larger horizontal displacements than in the no-slip case.

(c) Steady-state ice lens shapes

In steady state with $x^* < 1$, the polymer fraction field must satisfy

$$\frac{\partial^2 \Phi}{\partial {z^*}^2} = 0 \quad \text{so} \quad \Phi = r_1(x^*) + r_2(x^*)(z^* - a^*) \quad \text{with} \quad r_1(x^*) = 1 + \frac{1 + \cos \pi x^*}{2\mathcal{C}}, \tag{4.22}$$

from equations (4.8) and (4.9). Note also that $r_2(x^*) = \mathcal{M}\partial^2 \eta^*/\partial {z^*}^2$, using the flow boundary conditions, and so, since pervadic pressure gradients are not present in steady state, equation (4.14) shows that r_2 must be identically zero, since A and r_1 are functions of x^* alone. Hence, the steady-state polymer fraction field is simply a function of horizontal position, with

$$\Phi_\infty = 1 + \frac{1 + \cos \pi x^*}{2\mathcal{C}}. \tag{4.23}$$

When no-slip boundary conditions are imposed,

$$\eta^\infty_{\mathrm{NS}} = 2(1 - z)(\Phi_\infty^{1/2} - 1), \tag{4.24}$$

and so

$$a^*_\infty = \frac{2(\Phi_\infty^{1/2} - 1)}{1 + 2(\Phi_\infty^{1/2} - 1)} \approx \frac{1 + \cos \pi x^*}{\mathcal{C}} \tag{4.25}$$

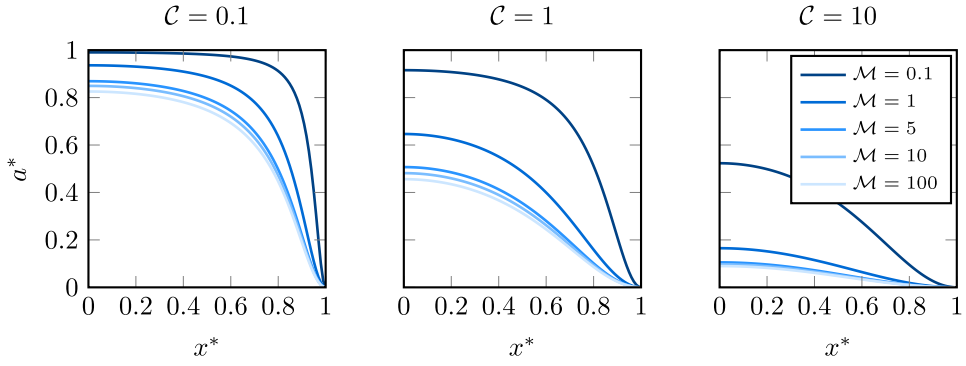

Figure 6: Plots of the steady state ice lens profile with free-slip boundary conditions defined in equation (4.27) for different values of $\mathcal{C}$ and $\mathcal{M}$.

in the large-$\mathcal{C}$ limit of LENS validity. In the case of free-slip boundary conditions, equation (4.10) shows that

$$\mathcal{M}\frac{\partial^2 \xi^*_{\mathrm{FS}}}{\partial {x^*}^2} = \frac{\partial \Phi_\infty}{\partial x^*}, \tag{4.26}$$

so, in the large-$\mathcal{C}$ regime,

$$a^*_\infty = \frac{2(\Phi_\infty^{1/2} - 1) + (\Phi_\infty - 1)/\mathcal{M}}{1 + 2(\Phi_\infty^{1/2} - 1) + (\Phi_\infty - 1)/\mathcal{M}}, \tag{4.27}$$

reducing to the same as in the no-slip case when $\mathcal{M}$ is large.

However, we can consider the freezing of significantly less stiff gels in the free-slip limit, as the requirement that $\mathcal{M} \gg 1$ need no longer be imposed. Figure 6 shows examples of the steady-state ice lens thickness as the parameters $\mathcal{C}$ and $\mathcal{M}$ are varied. In general, notice that larger values of $\mathcal{C}$ result in thinner ice lenses, since the gel must dry out to a lesser degree to lower the freezing temperature by a fixed amount. Larger values of $\mathcal{M}$ produce thinner ice lenses as well, as the deformation is resisted in the bulk of the gel by the formation of shear stresses.

(d) Transient ice growth

In order for growth to occur, water is driven from the bulk of the hydrogel into the ice layer via cryosuction, and our freezing model allows for these interstitial flows to be quantified. Since $\boldsymbol{u} = -(k/\mu_l)\boldsymbol{\nabla} p$,

$$\boldsymbol{u} = \frac{k\Pi_0}{\mu_l h}\left(\varepsilon\left[\frac{\partial \Phi}{\partial x^*} - \mathcal{M}\frac{\partial^2 \xi^*}{\partial {x^*}^2}\right], \frac{\partial \Phi}{\partial z^*} - \mathcal{M}\frac{\partial^2 \eta^*}{\partial {z^*}^2}\right), \tag{4.28}$$

illustrating how flows are vertical to leading order in the aspect ratio (downwards towards the growing ice layer) with an order-ε horizontal correction as flow is driven from more swollen to drier regions of the hydrogel. Figure 7 illustrates how the polymer fraction evolves in time and space as a result of the flow of interstitial fluid, with water drawn in from the bulk of the gel towards $x^* = 0$ and then downwards to the growing lens.

At very early times, the growth is approximately one-dimensional, with water drawn vertically downwards from a fully-swollen hydrogel. Therefore, we can approximate equation (4.9) by

$$\frac{\mathrm{d}a^*}{\mathrm{d}t^*} = \frac{Le}{2\mathcal{S}}\frac{1 + \cos \pi x^*}{a^*} \quad \text{so} \quad a^* \approx \sqrt{\frac{Le}{\mathcal{S}}\left(1 + \cos \pi x^*\right) t^*}. \tag{4.29}$$

As mentioned above, in the free-slip case, horizontal pressure gradients are small, and the bulk of fluid flows remain vertically-oriented, so this approximation holds for longer when the gel is not anchored at its edges.

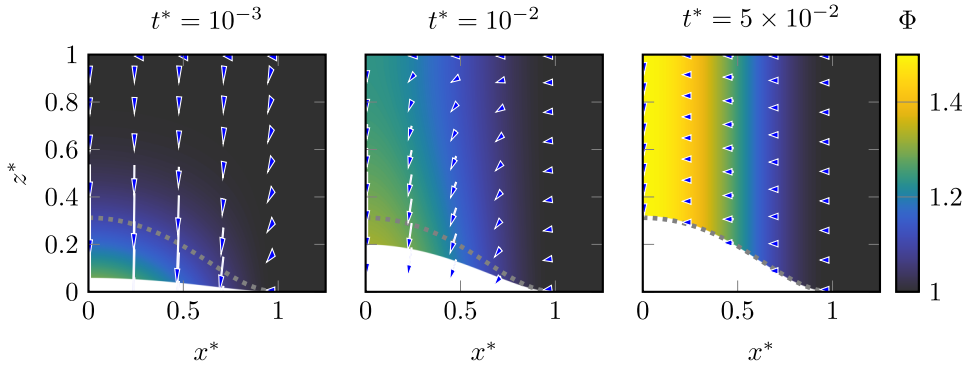

Figure 7: A contour plot of the polymer fraction field as the lower boundary of a gel with free-slip boundary conditions is cooled, showing the interstitial fluid velocity (arrows) and the approach to a steady-state ice lens (dotted curve). Here, $\mathcal{M} = 100$, $\mathcal{C} = 2$, $Le/\mathcal{S} = 10$ and $\varepsilon = 0.1$. At early times, ice is grown by drawing water vertically from the gel above it, whilst at later times water is primarily drawn longitudinally.

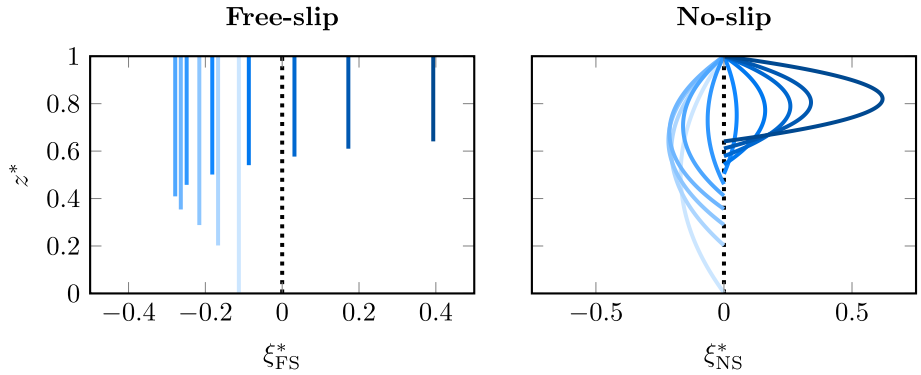

Figure 8: Plots of the horizontal displacement ξ^* at $x^* = 0.5$ for various times $t^* = 0$ to $t^* = 0.025$, with $\varepsilon = 0.1$, $\mathcal{M} = 10$, $\mathcal{C} = 0.1$ and $Le/\mathcal{S} = 10$. Time progresses from the lighter profiles to the darker ones, showing how the gel is initially pulled towards $x^* = 0$ (initial shrinkage) and then pushed away.

(e) Deformation of the gel

The approach to steady state is largely similar whether no-slip or free-slip boundary conditions are applied at the top surface, but the displacement field appears different in each case. Generally, there are two phases of deswelling seen as the ice layer grows and pushes the hydrogel out of place from the bottom left-hand corner. Initially, ice forms in a thin layer and dries out the hydrogel in immediate contact with the ice lens, causing a contraction in the polymer matrix and drawing polymer chains downwards and to the left as the scaffold shrinks. This is followed after some time by a regime where the dominant displacements are upwards and to the right, as the gel relaxes and is pushed out of the way.

It was shown in section 4(b) that our theory is only generally valid for both types of boundary condition in the limit of large $\mathcal{M}$ (gels where elastic 'stiffness' dominates over osmotic pressures) and large $\mathcal{C}$ (where there is a large depression in the liquidus temperature for a comparatively small deswelling of the gel). However, in the analysis that follows, we will use smaller values of

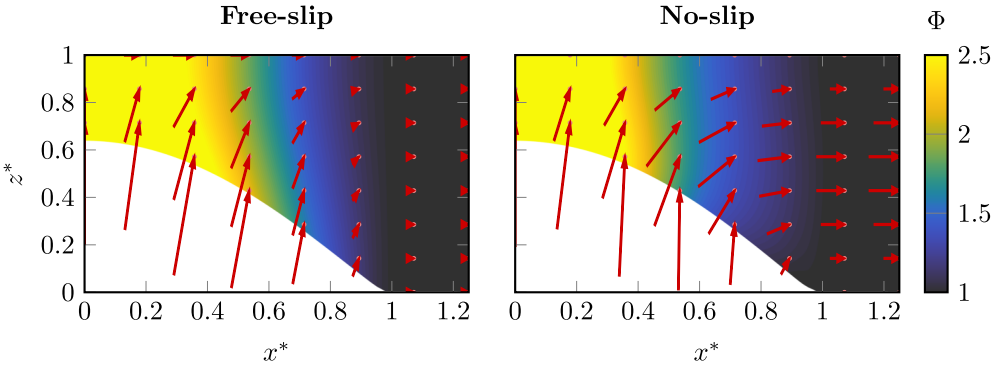

Figure 9: Plots of the displacement field at $t^* = 0.025$, with arrows from reference position to final position. The parameters $\varepsilon = 0.1$, $\mathcal{M} = 10$, $\mathcal{C} = 0.1$ and $Le/\mathcal{S} = 10$ are chosen to accentuate differences between the boundary conditions, even though they may result in solutions with large deviatoric strains, oustide of the range of validity of LENS theory.

$\mathcal{C}$ and $\mathcal{M}$ to produce results that are indicative of the qualitative behaviour for more nonlinear situations, even though such parameters may give rise to large deviatoric strains (as in figure 10) inconsistent with a LENS approach.

In figure 8, the evolution from negative to positive horizontal displacement is illustrated, showing also how displacements vary in the vertical direction. The initial shrinking behaviour is clear by the negative displacements at early times, which then become positive as the gel is forced rightwards by the growing ice.

Figure 9 shows the different displacement fields in this second phase of deswelling, with arrows marking the displacement of gel elements from an initial location at the base to a final position at the tip. Notice how the parabolic profile for ξ^*_{NS} is apparent in the no-slip case, and how the deformation appears more plug-like in the free-slip case where ξ^*_{FS} is independent of z^*.

In general, the presence of the ice lens displaces the gel to the right and upwards, but when free-slip conditions are applied, the horizontal displacement is seen to be independent of the z^* direction at leading order. We now investigate whether our model's predictions agree with the observations of [1] that lens formation is akin to the formation of a mode-I crack (i.e. dominated by stresses normal to the lens rupturing the gel by pushing it away) in the free-slip case, but akin to that of a mode-II crack (dominated by shear stresses formed at the peeling tip) in the no-slip case.

Our expressions for the displacement fields allow us to deduce leading-order approximations to the normal deviatoric strain ϵ_{zz} and the shearing strain ϵ_{xz}. Recalling the scalings from our lubrication assumption,

$$\epsilon_{zz} = \frac{\partial \eta^*}{\partial z^*} - 1 + \Phi^{1/2} \quad \text{and} \quad \epsilon_{xz} = \frac{1}{2}\left[\frac{1}{\varepsilon}\frac{\partial \xi^*}{\partial z^*} + \varepsilon \frac{\partial \eta^*}{\partial x^*}\right]. \tag{4.30}$$

If free-slip boundary conditions are applied, $\partial \xi^*/\partial z^* = 0$, and ϵ_{xz} is an order-ε quantity. Therefore, it is seen that normal strains (ϵ_{zz}) are much larger in this case, with

$$\epsilon_{zz} = 1 - \Phi^{1/2} - \frac{a^*}{1-a^*} + \frac{2}{1-a^*}\int_{a^*}^{1} \left(\Phi^{1/2} - 1\right) \mathrm{d}z' \quad \text{and} \quad \epsilon_{xz} = O(\varepsilon). \tag{4.31}$$

This shows that the formation of the ice lens affects the hydrogel in the same way that the opening of a mode-I (normal-stress-dominated) crack in the gel would, with the dominant displacement of material occuring normal to the forming ice lens. In the case of no-slip boundary conditions, the shear strains are order $1/\varepsilon$, compared with order-1 normal strains, and therefore the ice lens

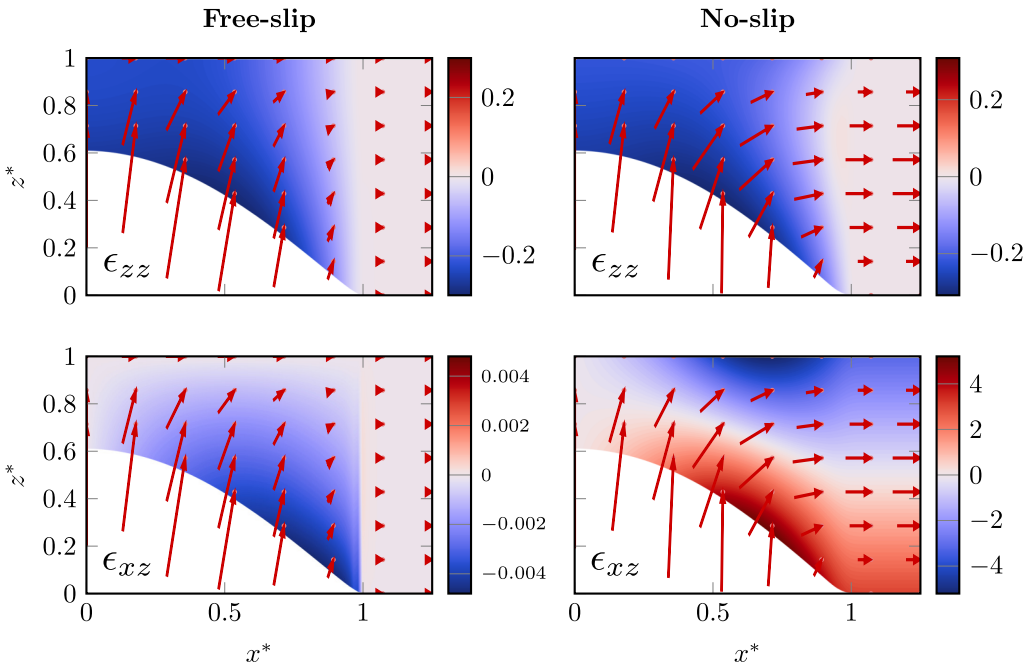

Figure 10: The normal (ϵ_{zz}) and shear (ϵ_{xz}) strain fields plotted for the two different boundary conditions at $t^* = 0.0225$ with the same parameters as figure 9. The red arrows represent displacements from equilibrium. Notice the different scales on the colour bars.

appears as a mode-II (shear-dominated) crack opening,

$$\epsilon_{zz} = 1 - \Phi^{1/2} + \frac{1-z^*}{2\mathcal{M}}\left[(z^*-a^*)\frac{\partial^2 \mathcal{P}}{\partial x^{*2}} - \frac{\partial a^*}{\partial x^*}\frac{\partial \mathcal{P}}{\partial x^*}\right] \quad \text{and}$$

$$\epsilon_{xz} = \frac{1}{\varepsilon}\frac{2z^* - (1+a^*)}{2\mathcal{M}}\frac{\partial \mathcal{P}}{\partial x^*} + O(\varepsilon). \tag{4.32}$$

In order to remain within the confines of LENS theory, all deviatoric strain components must be small, and therefore we are restricted to only modelling cases where a very thin ice layer ($a^* \ll 1$) forms with relatively little drying of the remaining gel ($\Phi \approx 1$). In this regime, ϵ_{xz} remains small in spite of the ε^{-1} prefactor, yet is still an order of magnitude larger than the normal strains.

Figure 10 shows the strain fields in both cases, illustrating the different ways in which the gel deforms as the ice lens forms. There is negative normal strain above the lens as the gel is compressed away from the lower boundary, with this normal stress higher in regions where more ice has grown. Above the ice lens, shearing strains are weakly negative in the free-slip case, reflecting that $\partial \xi^*/\partial z^*$ and $\partial \eta^*/\partial x^*$ are both less than zero. However, the parabolic horizontal displacement field leads to larger shear strains in the no-slip case, with both positive and negative shear above the ice lens. Again, note that the examples illustrated in this figure are deliberately chosen to give rise to large deviatoric strains for comparison purposes, even though solutions with large deviatoric strains lie outside the range of validity of the LENS model.

To illustrate this point, figure 11 plots the ratio of ϵ_{xz} to ϵ_{zz} as the gel deforms with the same material properties but different boundary conditions. It is clear that, in the free-slip case, the principal axes are aligned with the walls, but in the no-slip case there is a significant rotational component. In the free-slip case, normal strains are much greater than shear strains, and so we expect normal stresses to be larger in the gel. There are some shear stresses near the tip, as the crack opens wider (as would be expected), but everywhere the normal strains are at least an order of magnitude greater than shear. In the no-slip case, it is apparent that shear strains are

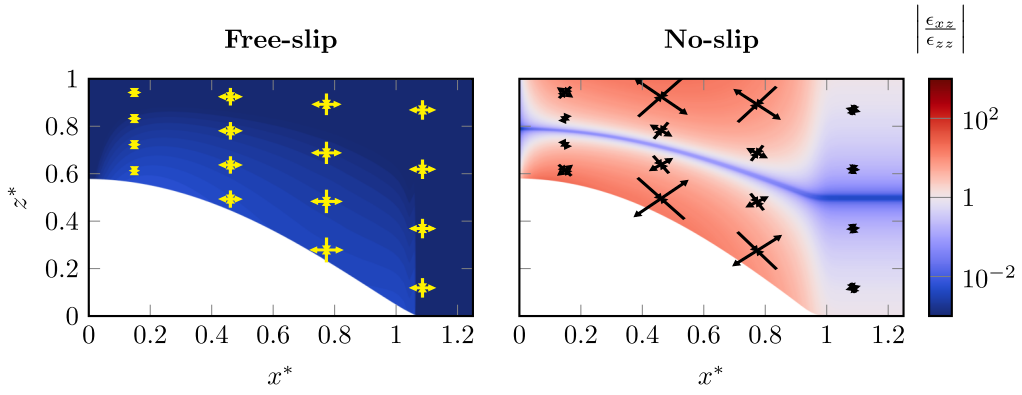

Figure 11: Plots of the ratio of shear to normal strain at $t^* = 0.02$ when applying free-slip or no-slip conditions on the top surface. The parameters are the same as in 9. Arrows indicate the principal axes and magnitude of the deviatoric strain tensor, with the direction indicating the nature of the strain (compressive or stretching). Notice the dominance of shear in the no-slip case.

larger than normal strains, since the horizontal displacement varies from a maximal value on the ice–gel interface to zero on the top surface. There are some normal stresses further away from the crack tip where the ice displaces the gel vertically upwards.

Our model does not, however, take into account the small amounts of expansion that occur as water freezes into ice. As discussed in the one-dimensional case, this inhibits the growth of an ice layer in a completely closed container, since expansion leads to arbitrarily high pressures that depress the freezing temperature of the water. In the formation of an ice lens, however, with a semi-infinite channel in the x direction, there could still be significant normal stresses imposed on the gel as it is compressed by the growing lens. These stresses could then lower the freezing temperature if they were to build up to a significant enough level such that the colligative assumption of equation (2.8) would no longer hold, especially in the case of no slip, where the gel would be displaced to the right as the ice grows but pinned in place on its top and bottom surface.

5. Conclusion

In this paper, we have applied our modelling of hydrogels to explain recent experimental observations of the freezing of such gels and to provide a complete description of the process of cryosuction, both by modelling the thermodynamic boundary conditions and the fluid flow through the polymer matrix induced by these interfacial effects. Though it has long been known that Gibbs-Thompson undercooling leads to the expulsion of water from a gel to form ice, and also that this process results in an elastic deformation of the polymer scaffold as water is lost, a coupled model of the hydrogel's deformation and the growth of ice has not yet, to our knowledge, been provided.

This process is driven by a boundary condition at the ice–gel phase boundary, which we discuss initially in the context of a one-dimensional model. This condition sets the liquidus temperature in terms of the osmotic pressure in the hydrogel, depressing the freezing point more for higher pressures. Alternatively, the same condition can be viewed as providing a boundary condition on the osmotic pressure given a temperature field, and it is this reverse view that is of more use in understanding the behaviour of the gel as the ice forms.

Swelling and drying processes typically start from an interfacial stress condition coupled with a condition on p that together set a value of Π at the edge of a gel. This cryosuction boundary condition leads to the flow of water from more swollen regions of the hydrogel to the interface, and drives the drying process as water is expelled into the ice. In finite-sized systems, a steady

state is eventually reached where the uniform osmotic pressure in the hydrogel is able to balance the undercooling effect in the Gibbs-Thompson relationship, and there is no further growth of ice. We showed above how this provides an alternative method for discerning the osmotic modulus of a gel sample without recourse to mechanical compression experiments, such as those outlined in [14]. A further avenue of research would be to compare the results of gel-freezing osmometry with mechanical compression experiments to check for agreement.

Then, we discussed the formation of 'ice lenses' at a cooled boundary with a temperature gradient. Much as in the one-dimensional case, ice grows by the expulsion of water from the hydrogel, with thicker ice at a cooler boundary, but the interfacial boundary condition now depends on the horizontal position x. This leads to greater drying of the hydrogel in the colder regions, and drives a flow parallel to the ice lens, replenishing the drier regions of the gel and driving further ice growth. This process couples complicated flow dynamics and deformation in the gel with a two-dimensional freezing problem, and so to model it analytically, we make the assumption of a small aspect ratio.

Under the lubrication approximation that the ice lens is much longer than it is thick, we were able to replicate many of the qualitative experimental observations made by [1]. Noticing that shear stresses are present at the crack tip with normal stresses more important behind this region, we are able to investigate the different effects of boundary conditions where the gel is fixed in place or free to slip on the stress patterns that result. Specifically, we have shown that the gel layer is deformed in a manner akin to a mode-II crack when the gel is bound to the top surface and like a mode-I crack when free to slip. This helps explain the source of stresses in the freezing hydrogel that result from cryosuction.

Acknowledgements. We thank Rob Style at ETH Zürich for a number of helpful discussions throughout the conception and development of this study, and for sharing the experimental data that motivated our investigation. JJW was supported by a Natural Environment Research Council studentship (project reference 2436164) through the Cambridge Climate, Life and Earth Sciences DTP (NE/S007164/1) and is now funded as part of the Leverhulme Trust Leadership Award 'Shape-Transforming Active Microfluidics' (RL-2019-014) to Tom Montenegro-Johnson at the University of Warwick.

References

1. Yang S, Gerber D, Feng Y, Bain N, Kuster M, de Lorenzis L, Xu Y, Dufresne ER, Style RW. 2024 Dehydration drives damage in the freezing of brittle hydrogels. *Sci. Adv.* **10**, eado7750. (10.1126/sciadv.ado7750)
2. Morelle XP, Illeperuma WR, Tian K, Bai R, Suo Z, Vlassak JJ. 2018 Highly stretchable and tough hydrogels below water freezing temperature. *Adv. Mater.* **30**, 1801541. (10.1002/adma.201801541)
3. Kuhn W, Peterli E, Majer H. 1955 Freezing point depression of gels produced by high polymer network. *J. Polym. Sci.* **16**, 539–548. (10.1002/pol.1955.120168238)
4. Worster MG. 2000 Solidification of Fluids. In *Perspectives in Fluid Dynamics* , . Cambridge University Press.
5. Dash JG, Rempel AW, Wettlaufer JS. 2006 The physics of premelted ice and its geophysical consequences. *Rev. Mod. Phys.* **78**, 695–741. (10.1103/RevModPhys.78.695)
6. Holmes DL, Stellwagen NC. 1991 Estimation of polyacrylamide gel pore size from Ferguson plots of normal and anomalously migrating DNA fragments. I. Gels containing 3% N,N'-methylenebisacrylamide. *Electrophoresis* **12**, 253–263. (10.1002/elps.1150120405)
7. Gerber D, Wilen LA, Poydenot F, Dufresne ER, Style RW. 2022 Stress accumulation by confined ice in a temperature gradient. *Proc. Natl. Acad. Sci. U. S. A.* **119**, e2200748119. (10.1073/pnas.2200748119)
8. Le Dizès Castell R, Sinaasappel R, Fontaine C, Smith SH, Kolpakov P, Bonn D, Shahidzadeh N. 2023 Frost damage in unsaturated porous media. *Phys. Rev. Appl.* **20**, 034025. (10.1103/PhysRevApplied.20.034025)
9. Tas RP, Sampaio-Pinto V, Wennekes T, van Laake LW, Voets IK. 2021 From the freezer to the clinic. *EMBO Reports* **22**, e52162. (https://doi.org/10.15252/embr.202052162)
10. Pearce RS. 2001 Plant Freezing and Damage. *Ann. Bot.* **87**, 417–424.

(https://doi.org/10.1006/anbo.2000.1352)
11. Dalvi-Isfahan M, Jha PK, Tavakoli J, Daraei-Garmakhany A, Xanthakis E, Le-Bail A. 2019 Review on identification, underlying mechanisms and evaluation of freezing damage. *J. Food Eng.* **255**, 50–60. (https://doi.org/10.1016/j.jfoodeng.2019.03.011)
12. Taber S. 1930 The mechanics of frost heaving. *J. Geol.* **38**, 303–317. (10.1086/623720)
13. Gerber D, Wilen LA, Dufresne ER, Style RW. 2023 Polycrystallinity enhances stress buildup around ice. *Phys. Rev. Lett.* **131**, 208201. (10.1103/PhysRevLett.131.208201)
14. Webber JJ, Worster MG. 2023 A linear-elastic-nonlinear-swelling theory for hydrogels. Part 1. Modelling of super-absorbent gels. *J. Fluid Mech.* **960**, A37. (10.1017/jfm.2023.200)
15. Webber JJ, Etzold MA, Worster MG. 2023 A linear-elastic-nonlinear-swelling theory for hydrogels. Part 2. Displacement formulation. *J. Fluid Mech.* **960**, A38. (10.1017/jfm.2023.201)
16. Feng Y, Gerber D, Heyden S, Kröger M, Dufresne ER, Isa L, Style RW. 2024 Characterizing hydrogel behavior under compression with gel-freezing osmometry. arXiv:2407.13718 [cond-mat] (10.48550/arXiv.2407.13718)
17. Peppin SSL, Elliott JAW, Worster MG. 2005 Pressure and relative motion in colloidal suspensions. *Phys. Fluids* **17**, 053301. (10.1063/1.1915027)
18. Peppin SSL. 2009 On diffusion and permeation. *J. Non-Equilib. Themodyn.* **34**, 355–369. (10.1515/JNETDY.2009.018)
19. Style RW, Gerber D, Rempel AW, Dufresne ER. 2023 The generalized Clapeyron equation and its application to confined ice growth. *J. Glaciol.* **69**, 1091–1096. (10.1017/jog.2023.28)
20. Nye JF. 1967 Theory of regelation. *Philos. Mag*, **16**, 1249–1266. (10.1080/14786436708229974)
21. Worster MG, Peppin SSL, Wettlaufer JS. 2021 Colloidal mushy layers. *J. Fluid Mech.* **914**, A28. (10.1017/jfm.2020.863)
22. Vlahou I, Worster MG. 2010 Ice growth in a spherical cavity of a porous medium. *J Glaciol.* **56**, 271–277. (10.3189/002214310791968494)
23. Brunner F, Seidlhofer T, Ulz MH. 2024 A numerical model for chemo-thermo-mechanical coupling at large strains with an application to thermoresponsive hydrogels. *Comput. Mech.* **74**, 509–536. (10.1007/s00466-024-02443-x)
24. Kaviany M. 1995 *Principles of Heat Transfer in Porous Media*. Springer. (10.1007/978-1-4612-4254-3)
25. Xu S, Cai S, Liu Z. 2018 Thermal conductivity of polyacrylamide hydrogels at the nanoscale. *ACS Appl. Mater. Interfaces* **10**, 36352–36360. (10.1021/acsami.8b09891)
26. Webber JJ. 2024 *Dynamics of super-absorbent hydrogels*. PhD thesis University of Cambridge.
27. Bertrand T, Peixinho J, Mukhopadhyay S, MacMinn CW. 2016 Dynamics of swelling and drying in a spherical gel. *Phys. Rev. Appl.* **6**, 064010. (10.1103/PhysRevApplied.6.064010)
28. Li J, Hu Y, Vlassak JJ, Suo Z. 2012 Experimental determination of equations of state for ideal elastomeric gels. *Soft Matt.* **8**, 8121–8128. (10.1039/C2SM25437A)
29. Etzold MA, Linden PF, Worster MG. 2021 Transpiration through hydrogels. *J. Fluid Mech.* **925**, A8. (10.1017/jfm.2021.608)
30. Irwin GR. 1957 Analysis of stresses and strains near the end of a crack traversing a plate. *J. Appl. Mech.* **24**, 361–364. (https://doi.org/10.1115/1.4011547)
31. Creton C, M. C. 2016 Fracture and adhesion of soft materials: a review. *Rep. Prog. Phys.* **79**, 044601. (10.1088/0034-4885/79/4/046601)